Supplementary Materials of

Exsolved medium-entropy alloy FeCoCuNi in titanate fibers enables solid oxide cells with superb electrochemical performance

Zilin Zhou,[a] Jiajia Cui, [a,b,*] Zhengrong Liu, [a] Jiaming Yang, [a] Yueyue Sun, [a] Chaofan Yin, [a] Zixuan Xue, [a] Jiaxi Niu, [a] Jingze Liu, [a] Kai Wu [a,*] and Jun Zhou [a,*]

[a.] *Center of Nanomaterials for Renewable Energy, State Key Laboratory of Electrical Insulation and Power Equipment, Xi'an Jiaotong University, Xi'an 710049, People's Republic of China.*

[b.] *School of Materials Science and Engineering, Xi'an University of Technology, Xi'an 710048, Shaanxi, People's Republic of China.*

The PDF file includes:

- Detailed preparation process of electrode
- Entropy calculation of multi-element alloy
- Faraday efficiency calculation
- Modeling of density functional theory calculation
- Reaction steps of co-electrolysis of CO_2 and H_2O
- Fig.S1. Section images of solid oxide cell
- Fig.S2. XRD and SEM images of LST fiber
- Fig.S3. Refined XRD images of LSTFCCN fiber
- Fig.S4. X-ray Photoelectron Spectroscopy (XPS) analysis of LSTFCCN fiber
- Fig.S5. Current-Voltage curve of LSTX cell under SOFC mode
- Fig.S6. Maximum power density of LSTX cell under SOFC mode
- Fig.S7. Short-time stability of LSTX cell under SOFC mode

- Fig.S8. Current-Voltage curve of LSTX cell under SOEC mode
- Fig.S9. Models of absorption energy calculation
- Fig.S10. Models of CO_2RR Gibbs free energy calculation
- Table.S1. Ratio of raw materials in LSTX fuel electrode preparation
- Table.S2. Lattice parameters of single-doped LSTX
- Tabld.S3. SOFC performance of single-doped LSTX electrode
- Table.S4. SOEC performance of single-doped LSTX cell
- Table.S5. Predicted adsorption energies for LST and LSTFCCN surfaces
- Table.S6. Specific Value of Atomic Bader Charge
- Table.S7. Comparison with SOEC/SOFC performance in other studies

Detailed preparation process of electrode

①Electrospinning: A series of $La_{0.4}Sr_{0.4}Ti_{0.9}X_{0.1}O_3$ (LSTX) nanofiber perovskite oxides with different concentrations of precursors PVP are prepared. Meanwhile, porous LSTX particles are prepared by sol-gel method for comparison, and the ratio is shown in Table.S1. According to the 0.004 mol target LSTX product, we weigh $La(NO_3)_3 \cdot 6H_2O$, $Sr(NO_3)_3 \cdot 6H_2O$, $Ni(NO_3)_3 \cdot 6H_2O$, $Fe(NO_3)_3 \cdot 6H_2O$, $Co(NO_3)_3 \cdot 6H_2O$, $Cu(NO_3)_2 \cdot 6H_2O$ and tetrabutyl titanate on the basis of stoichiometric ratio, and add them into appropriate amount of DMF solvent. A little acetic acid is also added to create a weak acid environment, and then an appropriate amount of PVP is added, and the mixed liquor is heated at 70 ℃ with magnetic stirring to obtain a transparent and viscous precursor solution. The electrospinning voltage is 15 kV, distance between needle and roller collector is 12 cm, and the injection speed is 3μl·min^{-1}.

②Synthesis of electrode materials: The obtained LSTX precursor fiber and the dry gel powder prepared by sol-gel method are transferred into a high-temperature box-type furnace. Firstly, the samples are heated to 400℃ at the rate of 1℃·min^{-1} and kept for an hour. Then the temperature is increased to 900 ℃ at a rate of 5 ℃·min^{-1}, kept for 3 hours and then cooled down at a rate of 5 ℃·min^{-1}.

③Preparation of cell: Firstly, appropriate amount of GDC powder is fully ball-milled with ethyl cellulose and terpineol solution for 24 hours to obtain GDC suspension. Secondly, the GDC suspension is evenly spun on the surface of SSZ electrolyte sheet. After spinning, SSZ electrolyte sheet is dried at 70 ℃ and then calcined at 1300 ℃ for 3 hours to obtain the electrolyte skeleton structure of "GDC|SSZ|GDC" initially. In the third step, terpineol and ethyl cellulose are fully mixed to make a viscous solution, while the electrode material powder and appropriate amount of solution are evenly ground to make a certain viscosity of the electrode material suspension. Through the screen pressing, the suspension is printed to the surface of the GDC layer and dried at 70℃, then being calcinated at 800 ℃ for 3 hours. Finally, we could obtain "electrode |GDC|SSZ|GDC|electrode" five-layer sandwich structured single cell.

Entropy calculation of multi-element alloy

According to Fig.2E, the entropy of FCCN alloy can be calculated as follows：

$$\Delta S_{Fe} = -0.1499 \times \ln 0.1499 = 0.2844$$

$$\Delta S_{Co} = -0.1546 \times \ln 0.1546 = 0.2886$$

$$\Delta S_{Ni} = -0.2526 \times \ln 0.2526 = 0.3476$$

$$\Delta S_{Cu} = -0.4429 \times \ln 0.4429 = 0.3607$$

$$\Delta S = \Delta S_{Fe} + \Delta S_{Co} + \Delta S_{Ni} + \Delta S_{Cu} = 1.2813$$

Entropy of FCCN alloy is higher than 1 and lower than 1.5, which means it is Medium-Entropy-Alloy.

Faraday efficiency calculation

Faraday efficiency is also calculated to characterize the electrolysis performance of LSTX cell, the equations are as follows:

$$FE_{CO} = \frac{\frac{v_{CO}}{1000 \cdot 22.4} \cdot 2 \cdot 96485}{I \cdot 60} = \frac{v_{CO}}{6.9648 \cdot I}$$

$$FE_{H_2} = \frac{\frac{v_{H_2}}{1000 \cdot 22.4} \cdot 2 \cdot 96485}{I \cdot 60} = \frac{v_{H_2}}{6.9648 \cdot I}$$

$$FE_{CH_4} = \frac{\frac{v_{CH_4}}{1000 \cdot 22.4} \cdot 8 \cdot 96485}{I \cdot 60} = \frac{v_{CH_4}}{1.7412 \cdot I}$$

$$S_{CH_4} = \frac{v_{CH_4}}{v_{CH_4} + v_{CO}}$$

$$T_{CO_2} = \frac{v_{CO} + v_{CH_4}}{v_{CO_2}}$$

Where: FE_{CO}: Faraday efficiency of CO

v_{CO}: volume of CO gas generated on each unit area at fuel electrode/ml·min^{-1}·cm^{-2}

I: current density/A·cm^{-2}

FE_{H_2}: Faraday efficiency of H_2

v_{H_2}: volume of H_2 gas generated on each unit area at fuel electrode/ml·min^{-1}·cm^{-2}

FE_{CH_4}: Faraday efficiency of CH_4

v_{CH_4}: volume of CH_4 gas generated on each unit area at fuel electrode/ml·min^{-1}·cm^{-2}

S_{CH_4}: selectance of CH_4

T_{CO_2}: conversion rate of CO_2

Modeling of density functional theory calculation

Firstly, the LST unit cell is modeled with a supercell model which contains 80 atoms ($La_8Sr_8Ti_{16}O_{48}$). Then the (110) surface slab is cleaved from the optimized supercell model of LST with O-terminations, and a 20 Å vacuum layer is attached to the upper surfaces of the slab. The FeCoCuNi atomic cluster is constructed on the upper surface of (110) surface slab to investigate the effects of FCCN alloys on the catalytic property on CO_2 reduction. Next, a CO_2 molecule with or without FeCoCuNi atomic cluster is adsorbed on the surface. In the case of LSTFCCN model, the CO_2 molecule is placed directly on the top of FCCN atomic cluster. For all structural optimizations, the atoms in the bottom layer of LST or LSTFCCN slab are fixed.

Reaction steps of electrolysis reaction of CO_2 and H_2O

$$CO_2(g) + H_2O(g) \rightarrow H_2(g) + CO(g) + CH_4(g) + O_2(g) \#(S1-1)$$

$$H_2O(g) + 2e^- \rightarrow H_2(g) + O^{2-} \#(S1-2)$$

$$CO_2(g) + 2e^- \rightarrow CO(g) + O^{2-} \#(S1-3)$$

$$H_2(g) + CO_2(g) \rightleftharpoons H_2O(g) + CO(g) \#(S1-4)$$

$$CO(g) + 3H_2(g) \rightleftharpoons CH_4(g) + H_2O(g) \#(S1-5)$$

$$C(s) + H_2O(g) \rightleftharpoons CO(g) + H_2(g) \#(S1-6)$$

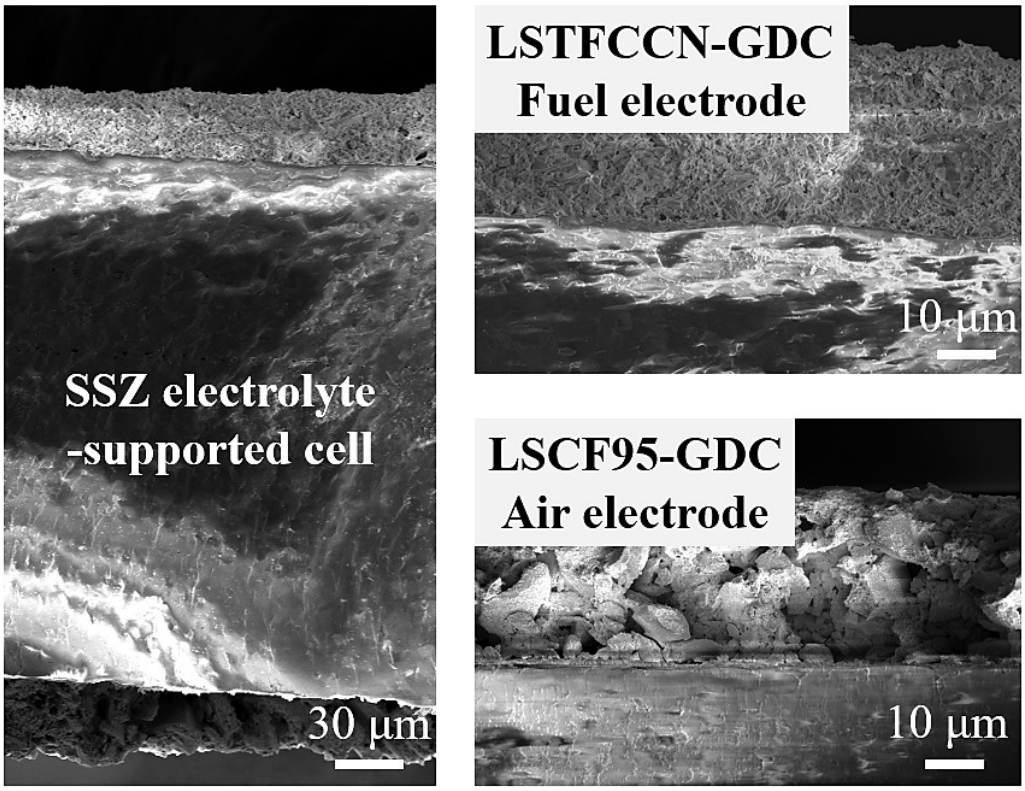

Fig.S1 SEM images of the cell's section.

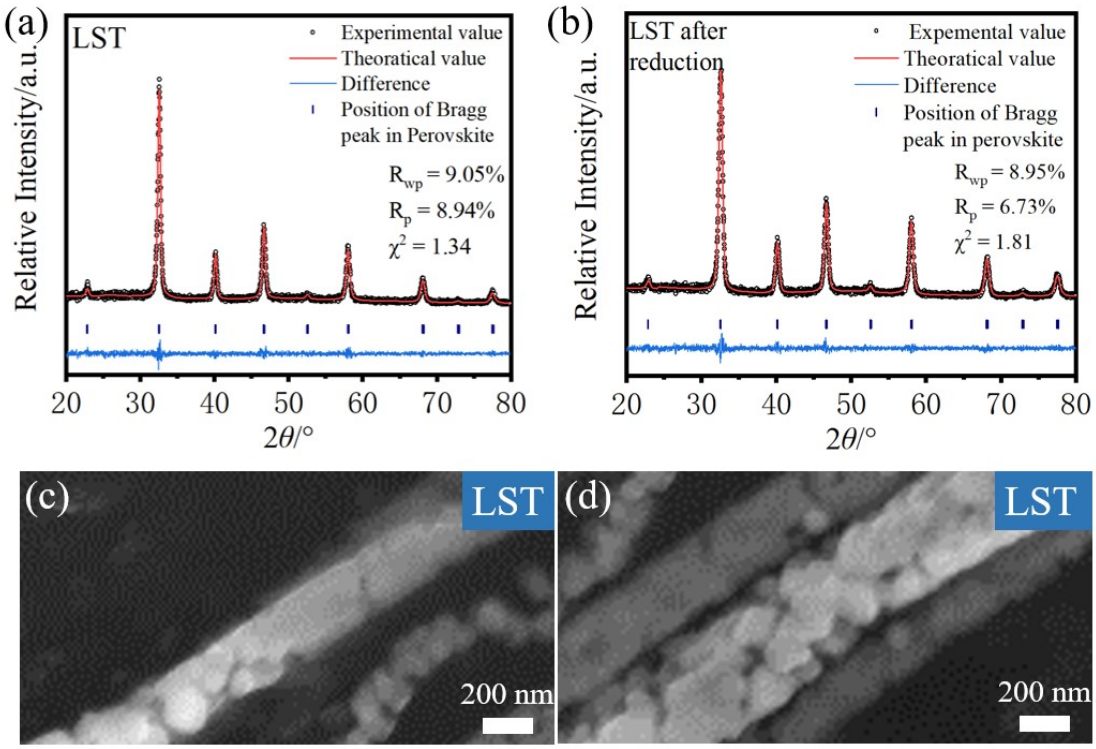

Fig.S2 (a)-(b) XRD analysis of LST fiber before and after reduction. (c)-(d) SEM images of LST fiber, the left one is the fiber before reduction, and the right one is the fiber after reduction.

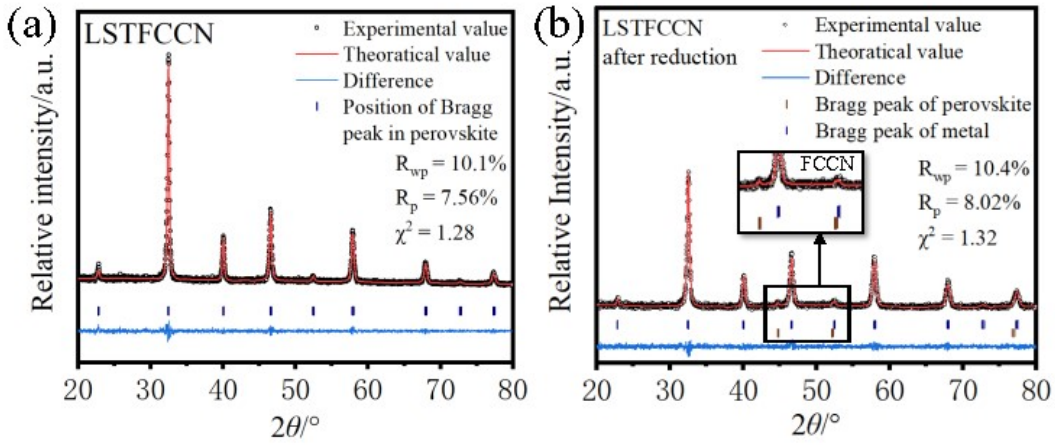

Fig.S3 (a)-(b) XRD analysis of LSTFCCN fiber before and after reduction.

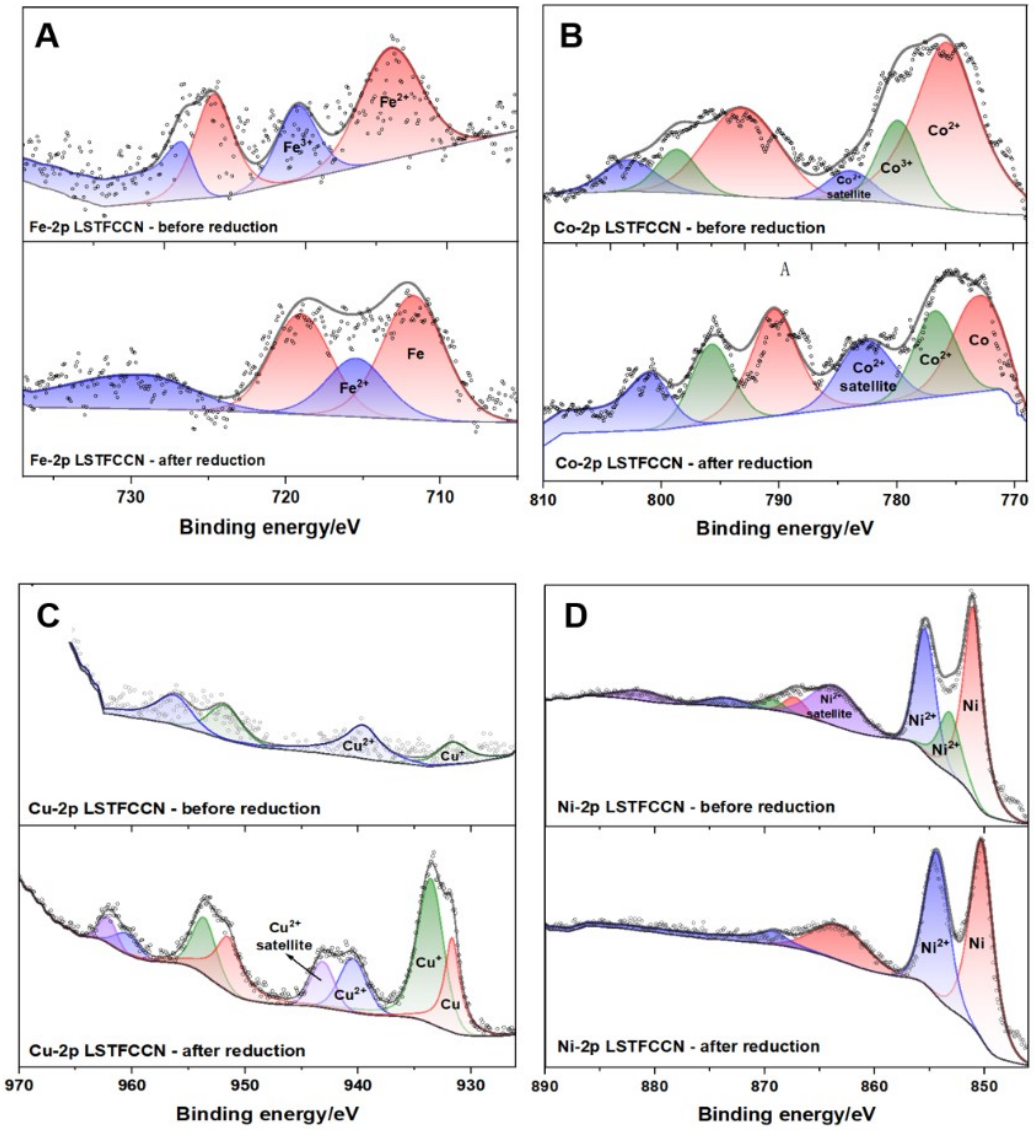

Fig.S4 X-ray Photoelectron Spectroscopy (XPS) analysis of LSTFCCN fiber

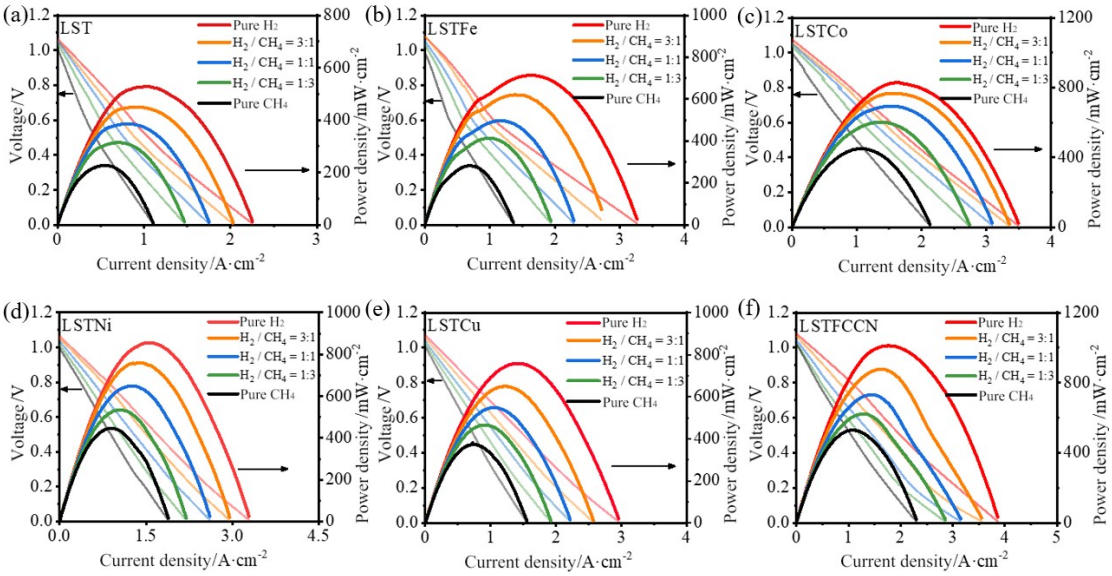

Fig.S5 Current-Voltage curve of LSTX cell under SOFC mode

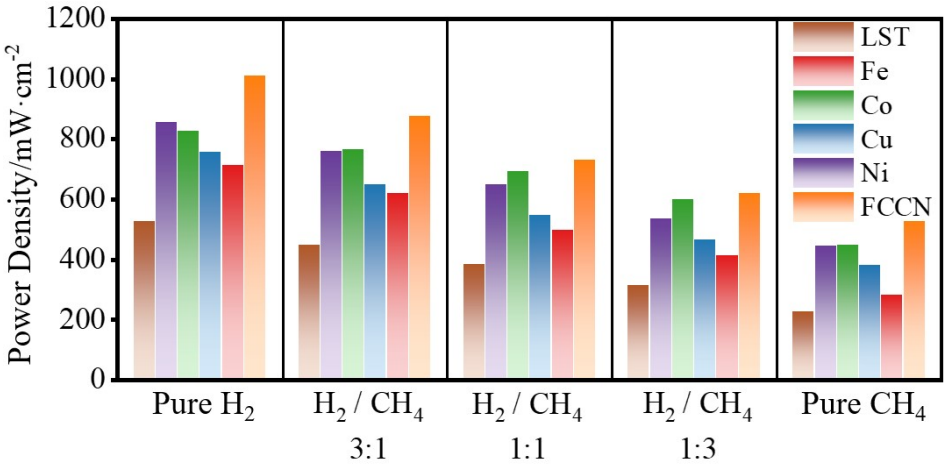

Fig.S6 Maximum power density of LSTX cell under SOFC mode

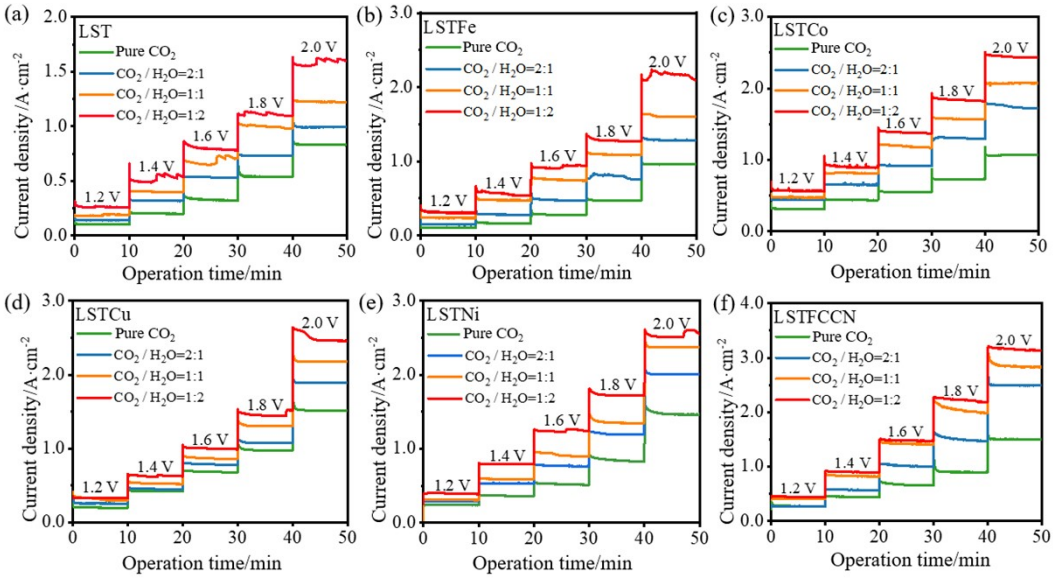

Fig.S7 Short-time stability of LSTX cell under SOFC mode

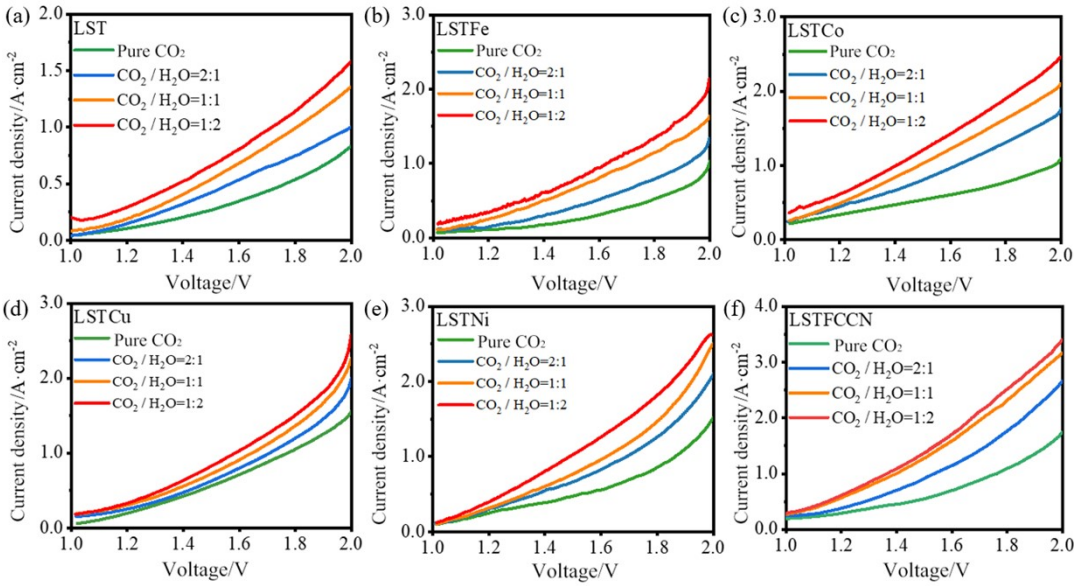

Fig.S8 Current-Voltage curve of LSTX cell under SOEC mode

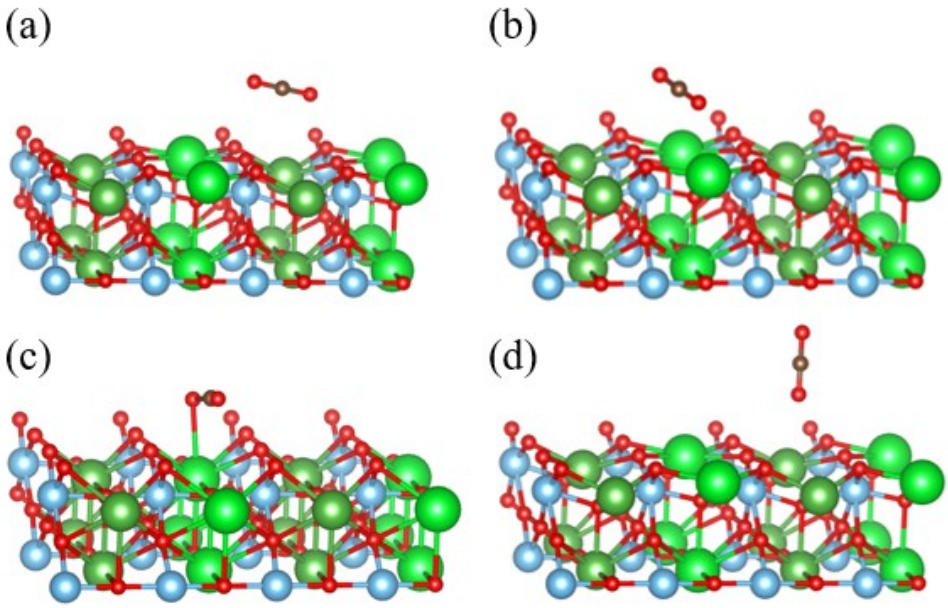

Fig.S9-1 Structures with different absorption sites after geometry optimization when only CO_2 was absorbed on surface. As for the bulk, light green balls are La atoms, deep green balls are Sr atoms, light blue balls are Ti atoms, brown balls are C atoms, and red balls are O atoms.

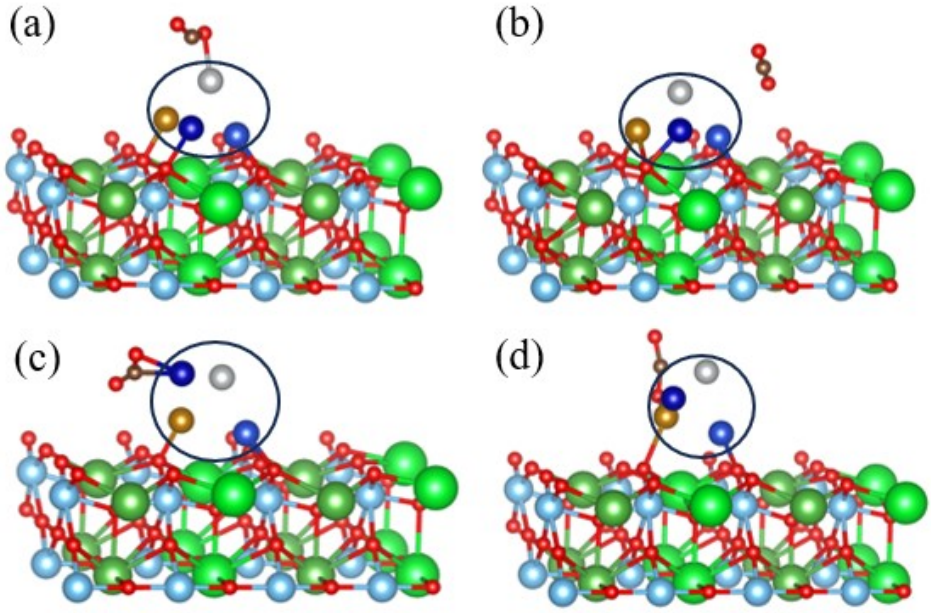

Fig.S9-2 Structures with different absorption sites after geometry optimization when cluster and CO_2 were co-absorbed on surface. As for the bulk, light green balls are La atoms, deep green balls are Sr atoms, light blue balls are Ti atoms, brown balls are C atoms, and red balls are O atoms. The 4 circled atoms form FCCN cluster.

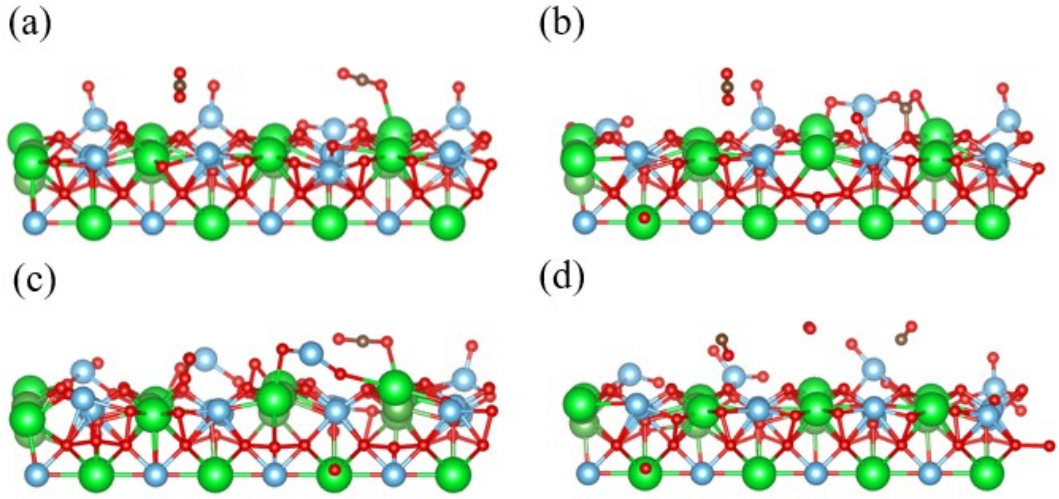

Fig.S10-1 Models of CO_2RR energy calculation (only CO_2 absorbed). As for the bulk, light green balls are La atoms, deep green balls are Sr atoms, light blue balls are Ti atoms, brown balls are C atoms, and red balls are O atoms.

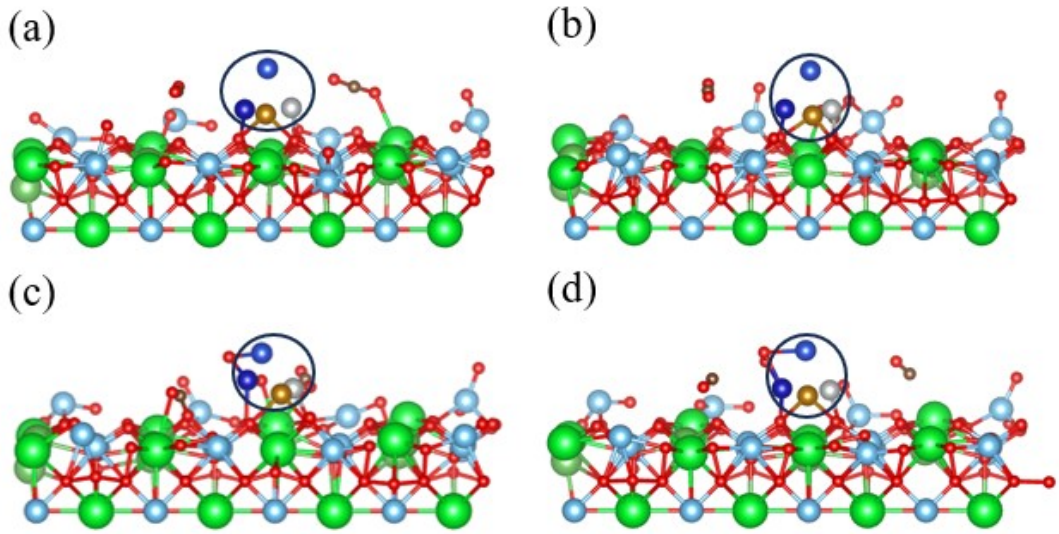

Fig.S10-2 Models of CO_2RR energy calculation (CO_2 and FCCN cluster co-absorbed). As for the bulk, light green balls are La atoms, deep green balls are Sr atoms, light blue balls are Ti atoms, brown balls are C atoms, and red balls are O atoms. The 4 circled atoms form FCCN cluster.

Tabel.S1 Ratio of raw materials in LSTX fuel electrode preparation

Fuel electrode	Concentration of PVP	Mass of PVP
LSTX particles	None (prepared by sol-gel method)	
LSTX7	7 wt%	0.85 g
LSTX10	10 wt%	1.26 g
LSTX13	13 wt%	1.69 g
LSTX16	16 wt%	2.16 g
LSTX13-GDC complex fiber electrode (mass ratio = 7:3)	13 wt%	1.69 g

Table.S2-1 Lattice parameters of LSTX fiber

Material	*a*/Å ($a = b = c$)	Space group
LST	3.89472	Pm-3m
LSTFe	3.89804	
LSTCo	3.90173	
LSTCu	3.90250	
LSTNi	3.89669	
LSTFCCN	3.89925	

Table.S2-2 Lattice parameters of LSTX fiber after reduction

Material	Content (mol ratio)	*a*/Å ($a = b = c$)	Space group
LST	100%	3.89598	Pm-3m
LSTFe	96.88%	3.90127	Pm-3m
Fe	3.12%	3.50817	Fm-3m
LSTCo	96.75%	3.90752	Pm-3m
Co	3.25%	3.53869	Fm-3m
LSTCu	93.14%	3.89593	Pm-3m
Cu	6.86%	3.61431	Fm-3m
LSTNi	95.57%	3.89239	Pm-3m
Ni	4.43%	3.49752	Fm-3m
LSTFCCN	95.41%	3.90210	Pm-3m
FeCoCuNi	4.59%	3.55284	Fm-3m

Table.S3-1 P_{Max} of LSTX cell under SOFC working mode

LSTX cell	Electrochemical Properties	Fuel gas				
		H_2	H_2 / CH_4 3:1	H_2 / CH_4 1:1	H_2 / CH_4 1:3	CH_4
LST	P_{Max}/mW·cm^{-2}	528	450	386	314	228
LSTFe		714	621	497	414	282
LSTCo		828	765	693	601	449
LSTCu		758	649	548	466	382
LSTNi		856	759	650	535	447
LSTFCCN		1011	877	731	622	529

Table.S3-2 R_p of LSTX cell under SOFC working mode

LSTX cell	Electrochemical Properties	Fuel gas				
		H_2	H_2 / CH_4 3:1	H_2 / CH_4 1:1	H_2 / CH_4 1:3	CH_4
LST	R_P/Ω·cm^2	0.302	0.377	0.457	0.536	0.780
LSTFe		0.206	0.265	0.330	0.416	0.551
LSTCo		0.128	0.173	0.219	0.316	0.425
LSTCu		0.187	0.237	0.294	0.367	0.438
LSTNi		0.143	0.176	0.211	0.286	0.383
LSTFCCN		0.111	0.161	0.192	0.226	0.311

Table.S4-1 Electrochemical performance of LSTX cell under SOEC working mode

LSTX cell	Fuel gas	Current density under 1.3V/A·cm^{-2}	Polarization resistance under different voltage/Ω·cm^2				
			1.1 V	1.2V	1.3V	1.4V	1.5V
LSTFe	CO_2	0.149	1.606	1.181	0.915	0.712	0.631
	2:1	0.228	1.356	0.982	0.789	0.579	0.486
	1:1	0.375	1.147	0.849	0.642	0.509	0.411
	1:2	0.478	0.839	0.694	0.429	0.370	0.325
LSTCo	CO_2	0.374	0.753	0.583	0.472	0.371	0.291
	2:1	0.525	0.583	0.405	0.285	0.258	0.220
	1:1	0.662	0.540	0.357	0.263	0.208	0.181
	1:2	0.794	0.359	0.287	0.216	0.180	0.163
LSTCu	CO_2	0.300	1.004	0.711	0.585	0.472	0.366

	2:1	0.306	0.928	0.670	0.529	0.439	0.357
	1:1	0.316	0.910	0.632	0.496	0.401	0.351
	1:2	0.370	0.866	0.609	0.459	0.384	0.330
LSTNi	CO_2	0.324	0.783	0.626	0.468	0.367	0.314
	2:1	0.416	0.607	0.491	0.402	0.335	0.303
	1:1	0.454	0.522	0.390	0.342	0.300	0.270
	1:2	0.591	0.467	0.358	0.301	0.268	0.229

Table.S5 Predicted adsorption energies for LST and LSTFCCN surfaces

System	E_{abs}/eV
$LaSrTi_2O_6$	-0.3099
$LaSrTi_2O_6 + FeCoNiCu$	-1.4808

Table.S6 Specific Value of Atomic Bader Charge

Atom	Charge	
	Single adsorbed	Co-adsorbed
C	0.000000	0.000001
O1	8.324242	8.017715
O2	8.004517	7.995289
Fe		15.447237
Co		16.587404
Ni		17.843711
Cu		10.575723

Table.S7 Comparison of performance with others' researches

Material	Power Density/W · cm^{-2}	Current Density/A · cm^{-2}	Experimental Conditions
LSTFCCN	**1.01**	**0.85**	
SBF[S1]	0.84	1.01	
PBC-BCW[RS2]	0.75	0.84	
NBCCF[S3]	0.94	0.92	SOFC mode: 800 ℃
(La/Sr)(Ti/Fe)O[S4]	0.70	0.52	SOEC mode: 1.3 V
PS30C[S5]	0.83	1.19	
PBNF0.1[S6]	0.65	0.90	

References:

S1 Zhang M, Du Z, Sun Z, et al. Unraveling the promotional role of $BaCO_3$ in the electrode reaction kinetics of an $SmBaFe_2O_{5+\delta}$ air electrode of reversible solid oxide cells[J]. Journal of Materials Chemistry A, 2023, 11(40): 21645-21654.

S2 Zhang M, Liu J, Du Z, et al. Highly active and stable oxygen electrode $PrBaCo_2O_{5+\delta}$-Ba_2CoWO_6 enabled by In Situ formed misfit dislocation interface for reversible solid oxide cell[J]. Applied Catalysis B: Environment and Energy, 2025, 361: 124669.

S3 Tian Y, Liu Y, Wang W, et al. High performance and stability of double perovskite-type oxide $NdBa_{0.5}Ca_{0.5}Co_{1.5}Fe_{0.5}O_{5+\delta}$ as an oxygen electrode for reversible solid oxide electrochemical cell[J]. Journal of Energy Chemistry, 2020, 43: 108-115.

S4 Zhang L, Li Y, Zhang B, et al. (La, Sr) (Ti, Fe) $O_{3-\delta}$ perovskite with in-situ constructed FeNi3 nanoparticles as fuel electrode for reversible solid oxide cell[J]. International Journal of Energy Research, 2021, 45(15): 21264-21273.

S5 Hu H, Wang C, Ni J, et al. Sr-Doped PrCrO3 with Intelligent $SrCrO_x$ Cocatalyst for the Fuel Electrode of Reversible Solid Oxide Cells[J]. ACS Sustainable Chemistry & Engineering, 2024, 12(10): 4051-4060.

S6 Li Z, Yang B, Qian B, et al. Evaluation of Fe-doped $Pr_{1.8}Ba_{0.2}NiO_4$ as a high-performance air electrode for reversible solid oxide cell[J]. Separation and Purification Technology, 2023, 308: 123002.